



Published in final edited form as:

J Biol Chem. 2004 December 17; 279(51): 53828–53839.

A Naturally Occurring Mutation of the Opsin Gene (T4R) in Dogs Affects Glycosylation and Stability of the G Protein-coupled Receptor*

Li Zhu^{a,b}, Geeng-Fu Jang^a, Beata Jastrzebska^{a,c}, Sławomir Filipek^d, Susan E. Pearce-Kelling^e, Gustavo D. Aguirre^f, Ronald E. Stenkamp^{c,g,h}, Gregory M. Acland^e, and Krzysztof Palczewski^{a,b,i,j}

a From the Department of Ophthalmology, University of Washington, Seattle, Washington 98195-6485

b From the Department of Chemistry, University of Washington, Seattle, Washington 98195-6485

c From the Department of Biological Structure University of Washington, Seattle, Washington 98195-6485

d International Institute of Molecular and Cell Biology, Warsaw PL-02109, Poland

e James A. Baker Institute for Animal Health, College of Veterinary Medicine, Cornell University, Ithaca, New York 14853-6401

f Department of Clinical Studies, School of Veterinary Medicine, University of Pennsylvania, Philadelphia, Pennsylvania 19104

g From the Department of Biochemistry, University of Washington, Seattle, Washington 98195-6485

h From the Department of Biomolecular Structure Center, University of Washington, Seattle, Washington 98195-6485

i From the Department of Pharmacology, University of Washington, Seattle, Washington 98195-6485

Abstract

Rho (rhodopsin; opsin plus 11-*cis*-retinal) is a prototypical G protein-coupled receptor responsible for the capture of a photon in retinal photoreceptor cells. A large number of mutations in the opsin gene associated with autosomal dominant retinitis pigmentosa have been identified. The naturally occurring T4R opsin mutation in the English mastiff dog leads to a progressive retinal degeneration that closely resembles human retinitis pigmentosa caused by the T4K mutation in the opsin gene. Using genetic approaches and biochemical assays, we explored the properties of the T4R mutant protein. Employing immunoaffinity-purified Rho from affected *RHO*^{T4R/T4R} dog retina, we found that the mutation abolished glycosylation at Asn², whereas glycosylation at Asn¹⁵ was unaffected, and the mutant opsin localized normally to the rod outer segments. Moreover, we found that T4R Rho* lost its chromophore faster as measured by the decay of *meta*-rhodopsin II and that it was less

*This work was supported in part by United States Public Health Service Grants EY01730, EY08061, EY13385, EY06855, EY13729, EY13132, GM63020, and EY13729 from the National Institutes of Health; an unrestricted grant from the Research to Prevent Blindness, Inc., New York (to the Department of Ophthalmology, University of Washington); a grant from the E. K. Bishop Foundation; the Van Sloun Fund for Canine Genetic Research; and Polish State Committee for Scientific Research Grant 3P05F02625. The costs of publication of this article were defrayed in part by the payment of page charges. This article must therefore be hereby marked "advertisement" in accordance with 18 U.S.C. Section 1734 solely to indicate this fact.

†To whom correspondence should be addressed: Dept. of Ophthalmology, University of Washington, 1957 NE Pacific St., P. O. Box 356485, Seattle, WA 98195-6485. Tel.: 206-543-9074; Fax: 206-221-6784; E-mail: palczews@u.washington.edu.

resistant to heat denaturation. Detergent-solubilized T4R opsin regenerated poorly and interacted abnormally with the G protein transducin (G_t). Structurally, the mutation affected mainly the “plug” at the intradiscal (extracellular) side of Rho, which is possibly responsible for protecting the chromophore from the access of bulk water. The T4R mutation may represent a novel molecular mechanism of degeneration where the unliganded form of the mutant opsin exerts a detrimental effect by losing its structural integrity.

G protein-coupled receptors constitute one of the most important families of signaling molecules in higher organisms and are also the largest class of cell-surface receptors (1,2). They represent the primary mechanism by which cells sense and respond to their external environment. Rho (rhodopsin), a representative member of the largest subfamily A (reviewed in Refs. 3-7), is the only G protein-coupled receptor whose crystal structure is known (8,9). Mutations of the genes encoding Rho are frequently associated with a number of pathological conditions inherited as autosomal dominant or autosomal recessive traits (10), classified into different classes based on biochemical properties (11,12).

Dominantly inherited diseases can result from (a) haploinsufficiency of a gene, (b) gain of novel function or uncontrolled activation, and (c) loss of function because of mutant protein misfolding and aggregation. The type of inheritance implies a strategy for potential intervention. For example, constitutive activity of K296E and K296M opsin mutants can be silenced by the addition of retinylamine analog inhibitors (13), whereas the misfolded protein for the P23H opsin mutant can be stabilized by retinoids, at least in a heterologous expression system (14,15). The disease-causing mutation T4K in opsin has been identified, but the molecular mechanism of the pathology caused by this mutant has not been elucidated (16). The prediction is that such a mutation will prevent the glycosylation at Asn², one of the two glycosylation sites in opsin. The effects of glycosylation on the retina and Rho functioning have been investigated previously (11,17-20). Tunicamycin, which inhibits the biosynthesis of *N*-acetylglucosaminylpyrophosphorylpolyisoprenol and thus prevents the formation of the Asn-linked oligosaccharides of glycoproteins, blocks the glycosylation of opsin *in vitro*, but only slightly decreases the polypeptide synthesis and intracellular transport of opsin (18,19). When expressed in a heterologous system, the T4K mutant displays increased mobility in SDS-PAGE experiments, suggesting that one or both sites (Asn² and/or Asn¹⁵) have not been glycosylated. The T4K mutant also regenerates poorly with 11-*cis*-retinal and displays low light-dependent activation of the rod photoreceptor G protein transducin (G_t) (11). The N2Q mutant has normal properties, whereas non-glycosylated Rho is ineffective in the G protein activation assay (19). After deglycosylation by peptide *N*-glycosidase F, Rho has spectral properties in the dark; and after bleaching, it retains properties similar to those of the native protein (20). When glycosylation at Asn² and Asn¹⁵ is prevented, Rho inserts properly into the phospholipid bilayer and can be regenerated with 11-*cis*-retinal (20,21). It also is properly synthesized and intracellularly transported (17), but its ability to carry out the light-dependent activation of G_t is diminished (19).

An opportunity to study the mechanism of retinitis pigmentosa (RP)¹ pathogenesis was presented when the T4R mutation was discovered in the English mastiff dog (22,23). The affected dogs display a dramatically slowed time course for recovery of rod photoreceptor function after light exposure and a distinctive topographic pattern of retinal degeneration (22). Here, we present the properties of T4R Rho isolated from the scarce native tissue. We conclude that mutation of opsin within the intradiscal region affects the stability of the protein and the regeneration of mutant Rho, but not its spectral properties. This study reveals that the

¹The abbreviations used are: RP, retinitis pigmentosa; DM, *n*-dodecyl β -*D*-maltoside; GTP γ S, guanosine 5'-*O*-(3-thiotriphosphate); bis-tris propane, 1,3-bis(tris(hydroxymethyl)aminopropane)propane.

molecule responsible for the retinal degeneration is opsin, suggesting yet another molecular mechanism for retinal degeneration.

EXPERIMENTAL PROCEDURES

Animals—All dogs (3–9 months old) studied were from a research colony of mixed-breed dogs maintained at the Retinal Disease Studies Facility (Kennett Square, PA). $RHO^{T4R/+}$ and $RHO^{T4R/T4R}$ dogs derive their mutant RHO allele from English mastiff dogs affected with autosomal dominant progressive retinal atrophy as described previously (22,23). $RPE65^{-/-}$ and $RPE65^{+/-}$ dogs derive their mutant allele, a 4-bp deletion in the canine $RPE65$ (retinal pigment epithelium protein of 65 kDa) gene, from a briard dog affected with the canine homolog of Leber's congenital amaurosis (24,25). All dogs used in this study were tested to determine their genotype at either or both the RHO (22,23) and $RPE65$ (25) loci as described previously. To produce $RHO^{T4R/+} RPE65^{-/-}$ double mutant dogs, an initial crossbreeding was undertaken between an affected female from the $RPE65^{-/-}$ strain (genotype $RHO^{+/+}RPE65^{-/-}$) and a heterozygous affected male from the $RHO^{T4R/+}$ strain (genotype $RHO^{T4R/+}RPE65^{+/+}$). One of their female progeny genotyped as $RHO^{T4R/+}RPE65^{+/-}$ was then backcrossed to an $RPE65^{-/-}$ male, yielding, among others, $RHO^{T4R/+}RPE65^{-/-}$ double mutant individuals.

Whole retinas were dissected from eyes enucleated immediately postmortem from dogs that had been dark-adapted for at least 15 h. The retinas were then immediately frozen in liquid nitrogen and maintained under cryogenic conditions until analyzed. All such procedures were undertaken under dim red illumination.

Materials—11-*cis*-Retinal was a gift from Dr. R. K. Crouch (University of South Carolina) through a contract with the National Institutes of Health. *n*-Dodecyl β -D-maltoside (DM) was purchased from Anatrace Inc. (Maumee, OH). GTP γ S was purchased from Sigma. Trypsin was purchased from Princeton Separation, Inc. (Adelphia, NJ). Monoclonal antibody 1D4 raised against the Rho C terminus was purchased from the National Cell Culture Center (Minneapolis, MN). Monoclonal antibody B6-30N raised against the Rho N terminus was a generous gift from Dr. P. A. Hargrave (University of Florida). The anti-G α monoclonal antibody was a generous gift from Dr. H. E. Hamm (Vanderbilt University Medical Center). The anti-G β polyclonal antibody was a generous gift from Dr. O. G. Kisselev (St. Louis University School of Medicine). The synthetic peptides were purchased from United Biochemical Research, Inc. (Seattle, WA). The amount of purified bovine G $_t$ was measured using a 2-D Quant kit (Amersham Biosciences). The hexyl-agarose resin was purchased from MP Biomedicals Inc. (Aurora, OH). Other resins and columns for chromatography were purchased from Amersham Biosciences.

Purification of Rho—Purified anti-Rho C terminus antibody 1D4 (26) was immobilized on CNBr-activated Sepharose 4B (27), and a 4.6 \times 12-mm column was packed with 2 mg of antibody 1D4/ml of Sepharose beads. All procedures employing Rho or retinoids were performed under dim red light unless mentioned otherwise. The dog retinas were homogenized in buffer containing 137 mM NaCl, 5.4 mM Na $_2$ HPO $_4$, 2.7 mM KCl, and 1.8 mM KH $_2$ PO $_4$ (pH 7.5) with a glass-to-glass homogenizer. Soluble proteins in the supernatant were removed by centrifugation at 14,000 \times g for 5 min, and the pellet was then solubilized in buffer containing 1% DM, 10 mM bis-tris propane, and 500 mM NaCl (pH 7.5). After centrifugation at 125,000 \times g for 20 min, the supernatant was loaded onto the antibody 1D4-packed immunoaffinity column, followed by thorough washing with buffer A (0.1% DM, 10 mM bis-tris propane, and 500 mM NaCl (pH 7.5)) at a flow rate of 0.5 ml/min. Finally, purified dog Rho was eluted with 100 μ M nonapeptide (TETSQVAPA) in buffer A at room temperature. The purified Rho concentration was determined using a Hewlett-Packard 8452A UV-visible spectrophotometer.

Electrophoresis and Immunoblotting—Protein separation was performed on 10% SDS-polyacrylamide gels. Coomassie Blue R-250 staining, silver staining, and immunoblotting (Immobilon-P polyvinylidene difluoride, Millipore Corp.) were carried out according to standard protocols. Antibodies 1D4 (26) and B6-30N (28) were used to detect the corresponding C-terminal and N-terminal epitopes. Alkaline phosphatase-conjugated goat anti-mouse IgG or goat anti-rabbit IgG (Promega) was used as a secondary antibody. Protein bands were visualized with the 5-bromo-4-chloro-3-indolyl phosphate/nitro blue tetrazolium color development substrate (Promega).

Deglycosylation of Rho—Peptide *N*-glycosidase F (New England Biolabs Inc.) was used for the Rho deglycosylation experiments. In brief, ~20 μ g of immunoaffinity-purified Rho was first denatured (according to the manufacturer's protocol) and incubated with 100 units of peptide *N*-glycosidase F at 37 °C for 14 h. Because deglycosylated Rho has a faster mobility on SDS-polyacrylamide gel (21), the samples were then immunoblotted with antibody 1D4 to confirm the completion of deglycosylation.

Quantification and Stability of Rho—Quantification of dog Rho was carried out spectrophotometrically. Whole dog retinas were homogenized with a glass-to-glass homogenizer. After centrifugation at 14,000 \times *g* for 5 min, the pellet was solubilized in buffer containing 1% DM, 10 mM bis-tris propane, and 150 mM NaCl (pH 7.5). The solubilized mixture was centrifuged at 125,000 \times *g* for 20 min, and one-fourth of the supernatant was used for quantification of the Rho concentration by UV-visible spectroscopy. In the stability experiments, UV-visible absorption spectra of freshly purified Rho samples were measured at 37 °C in the absence or presence of 20 mM NH₂OH (pH 7.0). The absorbance was recorded at 504 nm until it dropped below 30% of the initial reading. Standard deviations were calculated from three sets of data from parallel experiments.

Retinoid Analysis—Retinoids were extracted and derivatized as described previously (29-31). Samples were analyzed by normal-phase HPLC (Beckman Ultrasphere-Si HP1100 column, 5 μ m, 4.6 \times 250 mm) using an isocratic solvent system consisting of 0.5% (v/v) ethyl acetate in hexane for 15 min, followed by 4% ethyl acetate in hexane for 60 min at a flow rate of 1.4 ml/min at 20 °C. The diode array UV-visible detector was set at 325 nm. Data were analyzed with Hewlett-Packard Chemstation A.06.03 software.

Isolation of N-terminal Peptides for Mass Spectrometry Analysis—Immunoaffinity-purified dog T4R Rho was desalted with a D-Salt™ dextran desalting column (Pierce), and the original buffer was replaced with 50 mM NH₄HCO₃ (adjusted to pH 7.5). The fractions containing the majority of Rho were concentrated by lyophilization before SDS-PAGE analysis. After electrophoresis, the gel was first fixed with a solution of 50% EtOH and 10% AcOH for 1–2 h and then washed overnight with a solution of 50% MeOH and 10% AcOH. The washed gel was stained with a mixture of 0.02% Coomassie Blue R-250, 20% MeOH, and 10% AcOH and then destained with a solution of 50% MeOH and 10% AcOH. The protein bands corresponding to T4R Rho (~5 μ g in total) were excised into small pieces (~1 \times 1 \times 1 mm³) and extensively washed with a solution of 50% MeOH and 5% AcOH. After being dehydrated with CH₃CN and dried in a SpeedVac, the gel pieces were treated for 40 min with 10 mM dithiothreitol (DTT) in 50 mM NH₄HCO₃ at 40 °C. The solution was removed, and the gel pieces were rinsed with 50 mM NH₄HCO₃, dehydrated with CH₃CN, and dried again. The dried gel pieces were alkylated with 50 mM iodoacetamide in 50 mM NH₄HCO₃ for 40 min in the dark at 40 °C. After removal of the solution, the gel pieces were incubated with two rounds of 50 mM NH₄HCO₃ at room temperature for 10 min each time. Finally, the gel pieces were dehydrated with CH₃CN and digested for 24 h with 0.5 μ g of trypsin in 100 μ l of 50 mM NH₄HCO₃ at 37 °C. To extract the digested peptides, the solution was removed, and the digested gel pieces were incubated with another 100 μ l of 50 mM NH₄HCO₃ at room temperature

for 10 min. The incubation was repeated with two rounds of 50% CH₃CN and 5% AcOH and two rounds of 93% CH₃CN and 5% AcOH. The extracts were pooled, dried in a SpeedVac, and dissolved in 20 μ l of solvent A (1% CH₃CN and 0.2% AcOH) for liquid chromatography-tandem mass spectrometry (LC-MS/MS) analysis. In a parallel experiment, 10 μ g (7.5 nmol) of the synthetic N-terminal T4R Rho peptide Ac-MNGREGPNFYV was digested with 0.4 μ g of trypsin in 20 μ l of 50 mM NH₄HCO₃ at 37 °C for 18 h. The reaction was stopped by adding 0.8 μ l of AcOH, and the resulting mixture was dried in a SpeedVac and dissolved in solvent A to a final peptide concentration of 1 μ M for LC-MS/MS analysis.

Mass Spectrometry—Analysis of the tryptic N-terminal peptide Ac-MNGR (MH¹⁺, m/z 519.2354) was performed by microcolumn electrospray LC-MS/MS. The mass spectrometer (PE-Sciex API QSTAR PULSAR i Q-TOF) was coupled with a nebulization-assisted electrospray ionization source (PE-Sciex). The house-made microcolumn (250 μ m \times 15 cm) was prepared from fused silica tubing packed with Zorbax SB-C18 (4 μ m, 80 Å) using an inline microfilter as the column outlet frit. An Agilent 1100 series HPLC capillary pump was used to deliver a flow rate of 4 μ l/min with a gradient of 100% solvent A (0.2% AcOH) and 0% solvent B (90% CH₃CN and 0.2% AcOH) for 18 min and then gradually to 0% solvent A and 100% solvent B for another 50 min. Throughout the gradient, the mass spectrometer was programmed to monitor m/z in the range of 500–550 with a +1 charge only, followed by MS/MS (unit resolution) with three different preset values of collisional energy for each selected precursor ion. Similar results were obtained in two independent experiments.

Photosensitivity and Regeneration of the Visual Pigment—UV-visible absorption spectra of freshly purified dog Rho were first measured at 20 °C. The samples were then bleached at a 20-cm distance (to avoid overheating the sample) with a 60-watt light bulb for 10, 20, 30, and 300 s. Alternative bleaching was done using a long-pass wavelength filter (>490 nm). The results were comparable under both bleaching conditions. The UV-visible absorption spectra of the bleached samples were immediately measured after each bleaching. In the experiments without NH₂OH, H₂SO₄ was added after bleaching the sample for 5 min to adjust the final pH to 1.9 to trap the retinylidene Lys²⁹⁶. In another set of experiments, neutral NH₂OH was added to reach a final concentration of 20 mM before any bleaching was conducted. In the regeneration experiments, ~10 μ g of wild-type (WT) or T4R Rho solubilized in 1% DM or 2% digitonin was bleached thoroughly for 2 min with a Fiber-Lite illuminator at a distance of 15 cm. Next, 11-*cis*-retinal was added under dim red light, and the formation of Rho was measured immediately afterward. The final ratio of 11-*cis*-retinal to Rho was 50:1, which enabled fitting of the data to a pseudo first-order reaction ($P_{WT} < 0.0001$, $P_{T4R} < 0.0008$). The rate constants calculated for dog WT and T4R Rho were 0.00029 and 0.00001 s⁻¹, respectively.

Limited Proteolysis—Freshly purified dog WT and T4R Rho were quantified by UV-visible spectroscopy. Half of the samples were bleached by illumination with a Fiber-Lite illuminator for 5 min at room temperature in the presence of 20 mM neutral NH₂OH. Both Rho and the bleached opsin samples were digested at a 200:1 molar ratio of Rho to tosylphenylalanyl chloromethyl ketone-treated trypsin (Worthington) in buffer containing 137 mM NaCl, 5.4 mM Na₂HPO₄, 2.7 mM KCl, and 1.8 mM KH₂PO₄ (pH 7.5) for 5, 15, 30, or 45 min. The digestion was terminated by the addition of denaturing loading buffer (350 mM Tris-HCl, 350 mM SDS, 30% (v/v) glycerol, 600 mM dithiothreitol, and 175 μ M bromphenol blue), and the resulting mixture was immediately used for SDS-PAGE or immunoblot analysis.

Rates of meta-Rhodopsin II (Meta II) Decay—All measurements were performed with 0.1 nM dog Rho in a solution of 0.1% DM, 10 bis-tris propane, and 100 mM NaCl (pH 6.0), favoring the formation of Meta II. A PerkinElmer Life Sciences LS 50B luminescence spectrophotometer was used to measure the increase in intrinsic Trp fluorescence due to hydrolysis of the protonated Schiff base and release of all-*trans*-retinal from Rho (32-34).

Immunoaffinity-purified Rho was bleached with a Fiber-Lite illuminator for 15 s from a distance of 15 cm, immediately followed by fluorescence measurements. A thermostat was applied to stabilize the temperature of the cuvette at 20 °C during the measurement. Fluorometer slit settings were 2.5 μm at 295 nm for excitation and 8 μm at 330 nm for emission. Both fitted curves have R^2 values >0.99 .

Purification of G_r — G_t was extracted from fresh bovine rod outer segment (ROS) membranes. ROS from 200 bovine retinas were homogenized in 80 ml of ice-cold water. The membrane suspension was centrifuged at $45,000 \times g$ for 30 min, and the supernatant was collected. This extraction was repeated twice. The combined supernatant was centrifuged at $45,000 \times g$ for 30 min to remove ROS membrane contamination. The final supernatant was adjusted to contain 10 mM MOPS, 2 mM MgCl_2 , 1 mM DTT, and 0.5 mM benzamidine (pH 7.5). This solution was then loaded onto hexyl-agarose resin (10 \times 55 mm) equilibrated with buffer containing 10 mM MOPS (pH 7.5), 2 mM MgCl_2 , 1 mM DTT, and 0.5 mM benzamidine. Bound proteins were eluted by stepwise addition of 75 mM NaCl and then 300 mM NaCl in the equilibration buffer. Fractions eluted with 300 mM NaCl, containing G_t and phosphodiesterase, were dialyzed into 10 mM bis-tris propane, 100 mM NaCl, 1 mM DTT, and 0.5 mM benzamidine and used for preparing Rho*– G_t complexes. For the G_t activity assay, this protein was further separated from phosphodiesterase by size exclusion chromatography using a Superdex 200 10/300 GL column (10 \times 300 mm; Amersham Biosciences) equilibrated with 10 mM bis-tris propane (pH 7.5) containing 100 mM NaCl and 1 mM DTT (pH 7.5).

G_t Binding and Activation Assays—In the binding assay, affinity-purified dog Rho (WT or T4R mutant) was mixed with an equivalent amount of G_t in 10 mM bis-tris propane (pH 7.5) containing 100 mM NaCl, 1 mM MgCl_2 , 1 mM DTT, and 2 mM DM and then bleached and incubated for 15 min on ice to form the complex. To observe G_t dissociation in the other group of experiments, equivalent amounts of G_t and opsin were incubated in the same buffer with 100 μM $\text{GTP}\gamma\text{S}$ on ice for 30 min under room light before loading onto a size exclusion column. This chromatography was performed on a Superdex 200 10/300 GL column (10 \times 300 mm) at room temperature at a flow rate of 0.4 ml/min using 10 mM bis-tris propane (pH 7.5) containing 100 mM NaCl and 1 mM DTT. The protein concentration of each fraction was determined with a Cary 50 Bio UV-visible spectrophotometer (Varian Inc., Walnut Creek, CA), and the fractions were then analyzed by SDS-PAGE and immunoblotting as described above.

In the fluorescence assay of G_t activation, the ratio of G_t to Rho was $\sim 10:1$, with G_t at a concentration of 250 nM and Rho at 25 nM, within the linear range of fluorescence change and protein concentrations. The sample was bleached for 15 s using a Fiber-Lite covered with a long-pass wavelength filter (>490 nm), followed by a 10-min incubation (if not indicated otherwise) with continuous low speed stirring. The intrinsic fluorescence increase from $G\alpha_t$ was measured with the PerkinElmer Life Sciences LS 50B luminescence spectrophotometer employing excitation and emission wavelengths at 300 and 345 nm, respectively, as described (32-36). No signals from Rho in the absence of G_t were detected in the control experiment.

Histology and Immunocytochemistry—Canine retinas were prepared for morphological studies either by a triple fixation protocol (37) before embedding in plastic or by 4% paraformaldehyde fixation for cryosectioning and immunocytochemistry after optimal cutting temperature compound embedding. For immunocytochemical studies, sections from optimal cutting temperature compound-embedded retinas were labeled with monoclonal antibody K16-107C, directed against the C-terminal domain of opsin (provided by Dr. P. A. Hargrave) (28), and an anti-RPE65 peptide polyclonal antibody (provided by Dr. T. M. Redmond).

Modeling—Dog WT and mutant Rho models were built from the Protein Data Bank code 1HZX crystal structure. The loops not present in the Rho crystal structure were created using

the Modeler module (38) of Insight II Version 2000 (Accelrys, San Diego, CA). Verification of the created loops and of the whole structure was accomplished with the Profile-3D module (39) by evaluating the compatibility between sequence and structure. The resulting structures were embedded in dipalmitoylphosphatidylcholine membrane. Optimization of energy and molecular dynamics was conducted using the CVFF Forcefield in Insight II for both WT and T4R mutant Rho.

RESULTS

Mutation T4R—The T4R opsin mutation affects the region that is sequestered in the intradiscal space (Fig. 1A). The structures of WT and T4R Rho appear to be almost identical, as predicted from molecular dynamics (Fig. 1A). The T4R mutation does not influence the anchoring of Rho in the membrane because residue 4 is located very close to the intradiscal tip of Rho and is far from the membrane. Instead, Arg⁴ points its charged group outside Rho and interacts with the adjacent Glu⁵. The intradiscal surface in WT Rho is mostly negatively charged, and once mutated, the additional positive charge of Arg⁴ or differences in protein folding in the vicinity of this region prevent glycosylation at Asn² (Fig. 1A, *upper and middle panels, red*). The extracellular region of Rho is highly conserved among mammalian opsins, and a number of pathogenic mutations in mammals leading to autosomal dominant RP have been identified (Fig. 1B). Two sets of mutations will affect glycosylation at Asn² and Asn¹⁵ either by substitution of these residues with a residue that cannot be glycosylated or by elimination of consensus sequences that are essential for recognition by endoplasmic reticulum oligosaccharyltransferase. It is unclear how mutations in the intradiscal region affect oligomerization of Rho (Refs. 40-43; see also Ref. 4).

Mutant Opsin Accelerates Degeneration—Dog T4R opsin is more toxic to photoreceptor cells than Rho, as shown in the following genetic experiment. The absence of the retinal chromophore correlates with an increased toxicity of the protein. The fundus of the left eye of an 8-month-old affected *RHO*^{T4R/+} dog appeared to be within normal limits, with uniformly normal morphology and no ophthalmoscopic evidence of retinal degeneration (Fig. 2, *A1-A3*). It should be noted that older animals (>10 months) begin to exhibit severe retinal degeneration, initially in distinct topographic regions that later become more generalized (22). Fundus photomontages of the left eye of a 6.5-month-old *RHO*^{T4R/+} *RPE65*^{-/-} dog, which could not produce the chromophore because of mutation in the *RPE65* gene (24,25,44), displayed hyperreflectivity of the tapetal fundus (Fig. 2*B1*), moderate vascular attenuation, and changes characteristic of outer retinal thinning and mid-stage disease. This fundus appearance reflects the photoreceptor degeneration present uniformly throughout the double mutant retina, as shown in histological sections in Fig. 2 (*B2 and B3*).

***RHO*^{T4R/T4R} Dog Has a Normal Level of Visual Pigment**—Retinal immunocytochemistry of a 2-month-old homozygous affected *RHO*^{T4R/T4R} dog showed normal morphology and ROS formation (Fig. 3A). The retina from a *RHO*^{T4R/T4R} dog was employed to isolate Rho by affinity chromatography or retinoids by analytical techniques in our studies. UV-visible absorption spectra of immunoaffinity-purified WT and T4R Rho showed almost identical spectra and $A_{280\text{ nm}}/A_{500\text{ nm}}$ ratios of 1.70 and 1.72, respectively (Fig. 3B), suggesting that the mutation at this position does not affect the location of the intradiscal E2 loop of Rho, which comes close to the chromophore core (8,45). As assessed by silver staining, WT Rho and its mutant were purified to apparent homogeneity (Fig. 3B, *right panel*). The amounts of Rho as measured by UV-visible spectroscopy of complete extracts from dog retina in WT, *RHO*^{T4R/+}, and *RHO*^{T4R/T4R} eyes were comparable (Fig. 3B, *left panel, inset*). Similarly, the quantities of 11-*cis*-retinal, identified by specific elution time and spectral properties (29,30), in WT, *RHO*^{T4R/+}, and *RHO*^{T4R/T4R} retinal extracts were equal to values of 2.8, 2.65, and 2.5 nmol/eye, respectively (Fig. 3C, *upper panel, inset*). These results agree with the histological data.

The elevated all-*trans*-retinyl esters in the $RHO^{T4R/T4R}$ animal were within observed differences between individual dogs.

T4R Rho Is Not Glycosylated at Asn²—The glycosylation status of T4R Rho in extracted and purified Rho was evaluated by SDS-PAGE (Fig. 4A) and immunoblotting (data not shown). Rho from WT retina displayed a single band and predictably had two glycosylation sites; Rho from the $RHO^{T4R/+}$ retina had two bands indicating two forms of Rho, one with mobility equal to that of WT Rho and the other with higher mobility, suggesting only partial glycosylation. T4R Rho from $RHO^{T4R/T4R}$ retina displayed a single band, most likely only singly glycosylated Rho. When Rho from WT, $RHO^{T4R/+}$, and $RHO^{T4R/T4R}$ dogs was deglycosylated, the proteins had identical mobilities, which were somewhat faster than that of unmodified T4R Rho. All Rho samples moved faster after deglycosylation (Fig. 4B), suggesting that the Rho mutant is properly glycosylated at only a single site. Because the disease manifests regional differences in dog retina, we investigated whether there is a regional difference in the glycosylation. Immunoblotting of Rho from different quadrants showed very similar patterns (Fig. 4C), suggesting that there is no variability in glycosylation in the different sectors of the eye.

T4R Rho was in-gel digested with trypsin, and the released peptides were analyzed directly by LC-MS/MS. Interestingly, MS/MS data revealed that the standard and the sample gave m/z values of 520.1964 and 520.2368, respectively, corresponding to the Ac-MDGR peptide (calculated precursor ion monoisotopic mass for $[M + H]^+ = 520.2184$), which is the deaminated product of the authentic tryptic Ac-MNGR product (calculated monoisotopic mass for $[M + H]^+ = 519.2354$). Both MS/MS spectra were almost identical, and the y ions series (y_1 – y_4) could be fully observed together with some a ions and z ions or y ion- NH_3 (Fig. 5, A and B). The strongest evidence of the presence of Ac-MDGR instead of Ac-MNGR came from y_2 and y_3 , with the indication of the loss of a nominal mass of 115 Da (Asp). The observed fragmentation pattern is in agreement with the sequence Ac-MDGR. The same peptide was also identified with another trypsin from a different supplier (Worthington). Thus, this tryptic peptide is unexpectedly deaminated by trypsin. This does not change, however, the conclusion drawn from the analysis. Our results demonstrate clearly that the Asn residue in the second position of the T4R Rho mutant is not glycosylated.

T4R Rho Releases the Chromophore Faster than WT Rho—To study the release of retinal, immunoaffinity-purified WT Rho (Fig. 6, A and C) and T4R Rho (Fig. 6, B and D) were bleached in the presence and absence of NH_2OH . No significant differences were observed. However, when the chromophore was trapped in the protonated Schiff base linkage with H_2SO_4 , a smaller absorption peak was observed in the T4R Rho sample (~80% compared with WT Rho), suggesting that the chromophore after bleaching in T4R Rho was not as effectively retained in the binding site as in WT Rho (Fig. 6, A and B, *blue traces*).

We further measured the trapping of the chromophore in the binding site. The decay of Meta II was monitored (Fig. 7A) using a fluorescence assay that takes advantage of the increase in fluorescence when the chromophore leaves the binding pocket (32,34). Meta II of T4R Rho decayed faster in the presence and absence of NH_2OH than did Meta II of WT Rho (Fig. 7B). When the data were fitted to a first-order reaction, the time constants were calculated to be $\tau = 33.3$ min for WT Rho and $\tau = 12.2$ min for the mutant (Fig. 7C).

Dog mutant Rho was also less thermally stable than WT Rho (Fig. 8A). This difference in stability was diminished when a strong nucleophile (NH_2OH) was added (Fig. 8B). The lack of stability against NH_2OH is likely due to differences in the amino acid sequence within the chromophore-binding site of dog *versus* bovine Rho (Fig. 1B).

Regeneration in digitonin revealed another striking difference between dog WT and T4R Rho. In this detergent, T4R Rho regenerated slowly compared with WT Rho (Fig. 9). Similar differences were also observed in DM (data not shown). However, it should be noted that Rho regeneration took place *in vivo* in membranes (Fig. 3). The use of mild detergent may exacerbate the effect of mutation, uncovering more clearly the harmful effect of the mutation.

The Intradiscal Region of T4R Rho Is Less Structured—To investigate whether the intradiscal region is misfolded, limited proteolysis was employed. Trypsin cleaves the peptide bond at the C-terminal side of Arg or Lys when either is in an open configuration that can insert into the binding site of the protease. When Rho digestion was compared by SDS-PAGE and immunoblotting using anti-Rho C terminus and anti-Rho N terminus antibodies, major differences were observed (Fig. 10). WT Rho and T4R Rho lost only the C-terminal region as described previously (46) and were visualized by the anti-Rho N terminus antibody (doublet at ~36 kDa) (Fig. 10, B and E), as the C-terminal cleavage abolished recognition by the anti-Rho C terminus antibody (single band at ~36 kDa). In contrast to Rho, opsins were degraded much faster, as many low molecular mass species of the degraded proteins were observed. The N terminus of T4R opsin was digested much faster (Fig. 10E) than WT opsin (Fig. 10B). These differences could be a result of both the point mutation and the single glycosylation of T4R opsin. These results suggest that the N terminus is primarily affected, leading to the loss of recognition by the anti-Rho N terminus antibody.

Rho-G_t Binding and Activation*—Next, the interactions between G_t and WT or T4R Rho* were investigated (Fig. 11, A–C). Once formed, the Rho*-G_t complex had a higher molecular mass than either G_t or Rho itself and migrated faster through the size exclusion chromatography column. When run through the column alone, G_t eluted in fractions 35–43 (data not shown). In the G_t binding experiments, together with either bleached WT Rho or T4R Rho, G_t was mainly present in fractions 33 and 35 (Fig. 11A, upper panels), indicating that the complexes were formed. However, G_t was also present in fractions 37 and above, co-eluted with a proportional amount of opsin. In the presence of GTPγS (non-hydrolyzable analog of GTP), the dissociation of G_t from WT or T4R opsin was observed as G_t shifted toward the later fractions (fractions 37–39) (Fig. 11, A and B, lower panels). G_t dissociated more slowly from the T4R opsin complex than from the WT opsin complex, given the observation of the relative lag in the elution of G_t with T4R opsin. This suggests that the possible conformational change in the T4R mutant may play a role in either stronger binding or slower release.

In the G_t activation assay, which monitors the rate of change in intrinsic fluorescence from Gα_t (47,48), we obtained a much slower initial rate with T4R Rho* at either neutral or slightly acidic pH (Fig. 11C). WT Rho displayed a faster initial activation rate at neutral pH compared with slightly acidic pH, whereas the T4R mutant showed the opposite trend. The slower activation may be partially related to the faster decay of Meta II for the mutant. This observation was further supported by the experiment in which there was no GTPγS added until Rho* and G_t were incubated together for the measured relaxation time for the T4R mutant ($\tau = 12.2$ min). There was little or almost negligible increase in the fluorescence of Gα_t upon addition of GTPγS when Rho* decayed (Fig. 11C, gray trace). These results are consistent with the relaxation time measured; since most of the Meta II is consumed by that time, G_t activation is expected to be much slower. The apparent initial rates calculated from each group of experiments were as follows: WT Rho at pH 7.5, $k_0 = 0.0026$ s⁻¹; WT Rho at pH 6.0, $k_0 = 0.0019$ s⁻¹; T4R Rho at pH 6.0, $k_0 = 0.0013$ s⁻¹; T4R Rho at pH 7.5, $k_0 = 0.0005$ s⁻¹; and T4R Rho at 800 s > $\tau_{\text{Meta II}}$ at pH 7.5, $k_0 = 0.0003$ s⁻¹. Together, the lack of activation as measured by the fluorescence assay and the differences in the gel filtration of the complexes indicate that the T4R Rho*-G_t interaction is aberrant.

DISCUSSION

In this study, we investigated the properties of T4R Rho isolated from affected canine retinas; Rho was synthesized, processed, and trafficked in its native host cells, the rod photoreceptors. The main points of our experiments include the following. 1) The T4R mutation eliminates sites of recognition at Asn² by oligosaccharyltransferase throughout the dog retina, but it appears that Asn¹⁵ is glycosylated similarly compared with WT Rho. The lack of glycosylation at Asn² does not prevent transport of the mutant protein to ROS and its regeneration. The full complement of Rho is found in the dark-adapted animals. 2) The deleterious effect of the T4R mutation is likely mediated by opsin rather than by Rho. This difference, evident in multiple biochemical assays, was confirmed by the genetic experiment combining the T4R Rho mutation with the RPE65 knockout mutation. In double mutant dogs, the RPE65 mutation leads to a lack of chromophore production and greatly accelerated retinal degenerative disease compared with the single mutant T4R retina. 3) Mutation at the N terminus affects the chromophore-binding site, as the release of the chromophore is accelerated, and *in vitro* regeneration with 11-*cis*-retinal is inhibited; the mutation also affects formation of the active G_t conformation and the prompt release of activated G_t. It is clear that solubilization of Rho in mild detergent exacerbated these differences compared with native T4R Rho in membranes. However, the visual process happens repeatedly *in vivo*, whereas in the purified system, it is a one-time process. The lower thermal stability of the mutant may further aggravate the inherited instability of opsin *in vivo*.

Dog Versus Bovine Rho—As expected, the general properties of canine Rho studied here and bovine Rho from a number of previous studies were similar. The glycosylation of dog WT Rho was uniform as judged by SDS-PAGE, which is similar to that of bovine Rho isolated from retina. No differences in regeneration or glycosylation were observed in different parts of the dog retina. In contrast, Rho expressed in heterologous systems was heterogeneously glycosylated. Without any amino acid changes on the cytoplasmic surface implicated in binding G_t (49,50), dog WT Rho effectively stimulated bovine G_t. Bovine and dog Rho display similar bleaching properties, but due to nine changes within the chromophore-binding site (Fig. 1A, *lower panel*), the half-life for chromophore release is ~33 min for dog Rho (Fig. 7) compared with ~15 min for bovine Rho (Ref. 32 and confirmed in our assay). Dog Rho was less stable with respect to NH₂OH, again likely due to the differences in the amino acid residues within the chromophore-binding site.

In contrast, dog T4R Rho undergoes a different bleaching pathway, as the photoactivated mutant has a reduced ability to activate G_t, likely in part because its photoproduct corresponding to Meta II decays approximately three times faster compared with WT Rho. The binding of G_t to T4R Rho photoproduct(s) appears also to form an aberrant nonproductive complex that could be detrimental to the physiology of the photoreceptors and ultimately lead to their demise. The nature of the deviant interaction between G_t and the T4R mutant has not been explained at the mechanistic level or correlated with cell physiology in this study.

Structural Considerations—The electrostatic potential of the N-terminal region in WT Rho is negative due to the presence of Glu⁵. Introduction of Arg⁴ changes the positively charged distribution and may prevent glycosylation at Asn². However, it is somewhat surprising that the mutation on the intradiscal surface of the protein affects the chromophore-binding site and ultimately the cytoplasmic surface. We note that the P23H mutation on the intradiscal surface produces a hydrophilic channel in the interior of the protein that could accommodate water molecules and allow the hydrolysis of the covalently bound chromophore (14). Also, in the case of T4R, the chromophore appears to be destabilized by mutation in this general region. Both observations underscore the importance of the “plug” in maintaining the location of the chromophore and protecting it from hydrolysis (3).

In tissue culture, non-glycosylated opsin folds correctly as demonstrated by its normal palmitoylation, transport to the cell surface, and pigment formation with 11-*cis*-retinal (19). Similar to the T4R mutant described here, non-glycosylated Rho shows less efficient light-dependent activation of G_t. Using multiple substitutions that abolish glycosylation at Asn² and Asn¹⁵ and reduced G_t activation, it was suggested that glycosylation of Rho at Asn¹⁵ is more important in signal transduction (19). Additionally, it was correctly deduced that the extra-cellular region is involved in the formation of a specific structure, at present known as the plug (8). Bleaching of glycosylated and non-glycosylated Rho results in similar photo-bleached products as determined by absorption spectra, but non-glycosylated Rho is inefficient in G_t activation (19). Similarly for the dog T4R Rho mutants, the lack of glycosylation at Asn² and the introduction of the positive charge within this structurally sensitive region (Fig. 1A, *upper* and *middle panels*) are likely to be detrimental to protein stability and regeneration. Although bleaching appeared to be nearly normal, the signaling state of T4R Rho is clearly aberrant.

Congenital Night Blindness Versus RP Rho Mutants—Similar phenotypes as observed for dog T4R Rho could be more common and related to other Rho mutants characterized previously. Janz *et al.* (51) noticed an ion pair between Arg¹⁷⁷ and Asp¹⁹⁰, near the highly conserved disulfide bond in the extra-cellular region. This ion pair is found in almost all vertebrate opsins (Ref. 51; reviewed in Ref. 52). The ion pair opsin mutants regenerate with 11-*cis*-retinal and couple to G_t. However, they are thermally unstable in the dark state because of rapid hydrolysis of the retinal Schiff base linkage, indicating that the extracellular E2 loop encompassing this particular ion pair is important for Rho stability. This observation suggests that the Asp¹⁹⁰ mutant, observed in a subset of RP patients (53), may be thermally unstable and results in photoreceptor degeneration.

In addition, congenital night blindness mutants that are characterized by an open conformation of the chromophore-binding site for nucleophiles have been identified. For example, T94I opsin folds properly and binds 11-*cis*-retinal to form pigment, but T94I Rho displays reduced thermal stability, has a long lived Meta II photostate, and shows highly increased reactivity toward NH₂OH in the dark compared with WT Rho (54,55). In addition, it has been shown that T94I opsin is constitutively active (55). The abnormal function of this Rho mutant is likely related to the decreased thermal stability and opsin constitutive activity without protein misfolding. This property differentiates these and other congenital night blindness mutants (Refs. 55 and 56; reviewed in Ref. 57) from the structurally unstable mutants like T4R Rho described in this study or the previously mentioned RP Asp¹⁹⁰ Rho mutant (53). Interestingly, the most common RP mutant, P23H Rho, in addition to structural changes (14), is also less stable than the WT protein (15).

Potential Retinoid Supplementation and Lower Light Exposure May Counteract the RHO^{T4R} Mutant—As both the mouse and human age, there is a decline in the rate of Rho regeneration (reviewed by Jackson *et al.* (58)), which ultimately leads to photoreceptor loss (59). This process likely extends to dogs as well. Therefore, as the animal ages, more and more of the T4R opsin that is unstable will be generated, leading to progressive destruction of ROS disc structure. The defect is relatively mild, and only when a certain threshold is reached is there a sectorial massive degeneration. Based on the results obtained with double mutant animals that lack the enzymatic pathway for retinoid production through the retinoid cycle (reviewed by McBee *et al.* (60)), it is likely that light will further exacerbate the problem in the presence of the T4R mutation (Fig. 2). This would also apply to the T4K mutation, and lower light exposure and dietary supplementation with the photoactive chromophore may be therapeutic for RP patients with this class of mutations.

Interestingly, supplementation of 15,000 IU of vitamin A taken daily slows the progression of the common forms of RP as monitored by electroretinogram testing (61,62). Because of heterogeneity of the RP mutations, it was important to correlate these findings with specific amino acid substitutions. This study has been extended to the specific T17M Rho mutation. Li *et al.* (63) found that vitamin A supplementation slows the rate of photoreceptor degeneration in mutant mice carrying this Rho mutation. In addition, supplementation with *cis*-retinoids also improves cell targeting of P23H Rho under tissue culture conditions (14,15,64). Thus, this simple but potentially effective therapy deserves more attention and further improvements.

Novel Properties of Pathological Mutant Opsin—Opsin with a mutation that causes autosomal dominant RP may lead to an aberrant product that may, in turn, exhibit constitutive activity (65), have aberrant vectorial transportation (66), or misfold during biogenesis (14,64,67-69). The T4R mutation is characterized by opsin instability and may only manifest at a later stage of the disease when the supply of 11-*cis*-retinal is inhibited by the aging process or when the photoreceptors are exposed to intense light. We attribute these differences between the WT and T4R opsins to the positive charge at Arg⁴ resulting from the mutation and not the subsequent lack of glycosylation at Asn², as bovine deglycosylated Rho in our assays showed very similar properties to WT Rho. However, lack of glycosylation at Asn¹⁵ may cause other cell biological problems, as a substitution of Ser for Asn (N15S) was identified in a patient with autosomal dominant RP (70,71). In the case of human N15S and dog T4R mutations, the degeneration occurs within distinctive topographic regions (sectorial RP) (22,70-72) that could be related to differences in light exposure. Detailed analysis of patients with the T4K mutation is needed to further support this hypothesis.

Acknowledgments

We thank Dr. Vladimir Kuksa for valuable help with retinoid analyses; Amanda Nickle, Gerri Antonini, and the staff of the Retinal Disease Studies Facility; Julie Jordan and Pam Hammond for technical assistance; Keith Watamura for graphic support; Dr. R. K. Crouch for 11-*cis*-retinal; Dr. P. A. Hargrave for monoclonal antibody B6-30N; Dr. H. E. Hamm for anti-Gα_t antibody; Dr. T. M. Redmond for anti-RPE65 antibody; Dr. O. G. Kisselev for anti-Gβ_t antibody; and Rebecca Birdsong for help during manuscript preparation.

REFERENCES

1. Mirzadegan T, Benko G, Filipek S, Palczewski K. *Biochemistry* 2003;42:2759–2767. [PubMed: 12627940]
2. Pierce KL, Premont RT, Lefkowitz RJ. *Nat. Rev. Mol. Cell. Biol* 2002;3:639–650. [PubMed: 12209124]
3. Filipek S, Stenkamp RE, Teller DC, Palczewski K. *Annu. Rev. Physiol* 2003;65:851–879. [PubMed: 12471166]
4. Ridge KD, Abdulaev NG, Sousa M, Palczewski K. *Trends Biochem. Sci* 2003;28:479–487. [PubMed: 13678959]
5. Okada T, Ernst OP, Palczewski K, Hofmann KP. *Trends Biochem. Sci* 2001;26:318–324. [PubMed: 11343925]
6. Menon ST, Han M, Sakmar TP. *Physiol. Rev* 2001;81:1659–1688. [PubMed: 11581499]
7. Sakmar TP, Menon ST, Marin EP, Awad ES. *Annu. Rev. Biophys. Biomol. Struct* 2002;31:443–484. [PubMed: 11988478]
8. Palczewski K, Kumasaka T, Hori T, Behnke CA, Motoshima H, Fox BA, Le Trong I, Teller DC, Okada T, Stenkamp RE, Yamamoto M, Miyano M. *Science* 2000;289:739–745. [PubMed: 10926528]
9. Teller DC, Okada T, Behnke CA, Palczewski K, Stenkamp RE. *Biochemistry* 2001;40:7761–7772. [PubMed: 11425302]
10. Rattner A, Sun H, Nathans J. *Annu. Rev. Genet* 1999;33:89–131. [PubMed: 10690405]
11. Kaushal S, Khorana HG. *Biochemistry* 1994;33:6121–6128. [PubMed: 8193125]

12. Sung CH, Schneider BG, Agarwal N, Papermaster DS, Nathans J. *Proc. Natl. Acad. Sci. U. S. A* 1991;88:8840–8844. [PubMed: 1924344]
13. Yang T, Snider BB, Oprian DD. *Proc. Natl. Acad. Sci. U. S. A* 1997;94:13559–13564. [PubMed: 9391065]
14. Noorwez SM, Kuksa V, Imanishi Y, Zhu L, Filipek S, Palczewski K, Kaushal S. *J. Biol. Chem* 2003;278:14442–14450. [PubMed: 12566452]
15. Noorwez SM, Malhotra R, McDowell JH, Smith KA, Krebs MP, Kaushal S. *J. Biol. Chem* 2004;279:16278–16284. [PubMed: 14769795]
16. van den Born LI, van Schooneveld MJ, de Jong LA, Riemsdag FC, de Jong PT, Gal A, Bleeker-Wagemakers EM. *Ophthalmic Genet* 1994;15:51–60. [PubMed: 7850269]
17. Fliesler SJ, Rayborn ME, Hollyfield JG. *J. Cell Biol* 1985;100:574–587. [PubMed: 3155750]
18. Fliesler SJ, Rapp LM, Hollyfield JG. *Nature* 1984;311:575–577. [PubMed: 6332991]
19. Kaushal S, Ridge KD, Khorana HG. *Proc. Natl. Acad. Sci. U. S. A* 1994;91:4024–4028. [PubMed: 8171029]
20. Prasad AV, Plantner JJ, Kean EL. *Exp. Eye Res* 1992;54:913–920. [PubMed: 1521582]
21. Plantner JJ, Poncz L, Kean EL. *Arch Biochem. Biophys* 1980;201:527–532. [PubMed: 7396520]
22. Kijas JW, Cideciyan AV, Aleman TS, Pianta MJ, Pearce-Kelling SE, Miller BJ, Jacobson SG, Aguirre GD, Acland GM. *Proc. Natl. Acad. Sci. U. S. A* 2002;99:6328–6333. [PubMed: 11972042]
23. Kijas JW, Miller BJ, Pearce-Kelling SE, Aguirre GD, Acland GM. *J. Hered* 2003;94:27–30. [PubMed: 12692159]
24. Acland GM, Aguirre GD, Ray J, Zhang Q, Aleman TS, Cideciyan AV, Pearce-Kelling SE, Anand V, Zeng Y, Maguire AM, Jacobson SG, Hauswirth WW, Bennett J. *Nat. Genet* 2001;28:92–95. [PubMed: 11326284]
25. Aguirre GD, Baldwin V, Pearce-Kelling S, Narfstrom K, Ray K, Acland GM. *Mol. Vis* 1998;4:23–29. [PubMed: 9808841]
26. Molday RS, MacKenzie D. *Biochemistry* 1983;22:653–660. [PubMed: 6188482]
27. Oprian DD, Molday RS, Kaufman RJ, Khorana HG. *Proc. Natl. Acad. Sci. U. S. A* 1987;84:8874–8878. [PubMed: 2962193]
28. Adamo G, Zam ZS, Arendt A, Palczewski K, McDowell JH, Hargrave PA. *Vision Res* 1991;31:17–31. [PubMed: 2006550]
29. Van Hooser JP, Liang Y, Maeda T, Kuksa V, Jang G-F, He YG, Rieke F, Fong HK, Detwiler PB, Palczewski K. *J. Biol. Chem* 2002;277:19173–19182. [PubMed: 11897783]
30. Van Hooser JP, Aleman TS, He YG, Cideciyan AV, Kuksa V, Pittler SJ, Stone EM, Jacobson SG, Palczewski K. *Proc. Natl. Acad. Sci. U. S. A* 2000;97:8623–8628. [PubMed: 10869443]
31. Maeda T, Van Hooser JP, Driessen CA, Filipek S, Janssen JJ, Palczewski K. *J. Neurochem* 2003;85:944–956. [PubMed: 12716426]
32. Farrens DL, Khorana HG. *J. Biol. Chem* 1995;270:5073–5076. [PubMed: 7890614]
33. Schadel SA, Heck M, Maretzki D, Filipek S, Teller DC, Palczewski K, Hofmann KP. *J. Biol. Chem* 2003;278:24896–24903. [PubMed: 12707280]
34. Heck M, Schadel SA, Maretzki D, Bartl FJ, Ritter E, Palczewski K, Hofmann KP. *J. Biol. Chem* 2003;278:3162–3169. [PubMed: 12427735]
35. Farrens DL, Altenbach C, Yang K, Hubbell WL, Khorana HG. *Science* 1996;274:768–770. [PubMed: 8864113]
36. Fahmy K, Sakmar TP. *Biochemistry* 1993;32:9165–9171. [PubMed: 8396426]
37. Acland GM, Aguirre GD. *Exp. Eye Res* 1987;44:491–521. [PubMed: 3496233]
38. Sali A, Potterton L, Yuan F, van Vlijmen H, Karplus M. *Proteins* 1995;23:318–326. [PubMed: 8710825]
39. Bowie JU, Luthy R, Eisenberg D. *Science* 1991;253:164–170. [PubMed: 1853201]
40. Fotiadis D, Liang Y, Filipek S, Saperstein DA, Engel A, Palczewski K. *FEBS Lett* 2004;564:281–288. [PubMed: 15111110]
41. Filipek S, Krzysko KA, Fotiadis D, Liang Y, Saperstein DA, Engel A, Palczewski K. *Photochem. Photobiol. Sci* 2004;3:628–638. [PubMed: 15170495]

42. Fotiadis D, Liang Y, Filipek S, Saperstein DA, Engel A, Palczewski K. *Nature* 2003;421:127–128. [PubMed: 12520290]
43. Liang Y, Fotiadis D, Filipek S, Saperstein DA, Palczewski K, Engel A. *J. Biol. Chem* 2003;278:21655–21662. [PubMed: 12663652]
44. Redmond TM, Yu S, Lee E, Bok D, Hamasaki D, Chen N, Goletz P, Ma JX, Crouch RK, Pfeifer K. *Nat. Genet* 1998;20:344–351. [PubMed: 9843205]
45. Teller DC, Stenkamp RE, Palczewski K. *FEBS Lett* 2003;555:151–159. [PubMed: 14630336]
46. Palczewski K, Buczylo J, Kaplan MW, Polans AS, Crabb JW. *J. Biol. Chem* 1991;266:12949–12955. [PubMed: 2071581]
47. Heck M, Hofmann KP. *J. Biol. Chem* 2001;276:10000–10009. [PubMed: 11116153]
48. Ernst OP, Bieri C, Vogel H, Hofmann KP. *Methods Enzymol* 2000;315:471–489. [PubMed: 10736721]
49. Hargrave PA, Hamm HE, Hofmann KP. *BioEssays* 1993;15:43–50. [PubMed: 8466475]
50. Janz JM, Farrens DL. *J. Biol. Chem* 2004;279:29767–29773. [PubMed: 15070895]
51. Janz JM, Fay JF, Farrens DL. *J. Biol. Chem* 2003;278:16982–16991. [PubMed: 12547830]
52. Janz JM, Farrens DL. *Vision Res* 2003;43:2991–3002. [PubMed: 14611935]
53. Sung CH, Davenport CM, Hennessey JC, Maumenee IH, Jacobson SG, Heckenlively JR, Nowakowski R, Fishman G, Gouras P, Nathans J. *Proc. Natl. Acad. Sci. U. S. A* 1991;88:6481–6485. [PubMed: 1862076]
54. Ramon E, del Valle LJ, Garriga P. *J. Biol. Chem* 2003;278:6427–6432. [PubMed: 12466267]
55. Gross AK, Rao VR, Oprian DD. *Biochemistry* 2003;42:2009–2015. [PubMed: 12590588]
56. Gross AK, Xie G, Oprian DD. *Biochemistry* 2003;42:2002–2008. [PubMed: 12590587]
57. Abdulaev NG. *Trends Biochem. Sci* 2003;28:399–402. [PubMed: 12932725]
58. Jackson GR, Owsley C, Curcio CA. *Ageing Res. Rev* 2002;1:381–396. [PubMed: 12067593]
59. Curcio CA, Medeiros NE, Millican CL. *Investig. Ophthalmol. Vis. Sci* 1996;37:1236–1249. [PubMed: 8641827]
60. McBee JK, Palczewski K, Baehr W, Pepperberg DR. *Prog. Retin. Eye Res* 2001;20:469–529. [PubMed: 11390257]
61. Berson EL, Rosner B, Sandberg MA, Hayes KC, Nicholson BW, Weigel-DiFranco C, Willett W. *Arch. Ophthalmol* 1993;111:1456–1459. [PubMed: 8240091]
62. Berson EL, Rosner B, Sandberg MA, Hayes KC, Nicholson BW, Weigel-DiFranco C, Willett W. *Arch. Ophthalmol* 1993;111:761–772. [PubMed: 8512476]
63. Li T, Sandberg MA, Pawlyk BS, Rosner B, Hayes KC, Dryja TP, Berson EL. *Proc. Natl. Acad. Sci. U. S. A* 1998;95:11933–11938. [PubMed: 9751768]
64. Saliba RS, Munro PM, Luthert PJ, Cheetham ME. *J. Cell Sci* 2002;115:2907–2918. [PubMed: 12082151]
65. Jin S, Cornwall MC, Oprian DD. *Nat. Neurosci* 2003;6:731–735. [PubMed: 12778053]
66. Sung CH, Makino C, Baylor D, Nathans J. *J. Neurosci* 1994;14:5818–5833. [PubMed: 7523628]
67. Illing ME, Rajan RS, Bence NF, Kopito RR. *J. Biol. Chem* 2002;277:34150–34160. [PubMed: 12091393]
68. Chapple JP, Cheetham ME. *J. Biol. Chem* 2003;278:19087–19094. [PubMed: 12754272]
69. Roof DJ, Adamian M, Hayes A. *Investig. Ophthalmol. Vis. Sci* 1994;35:4049–4062. [PubMed: 7960587]
70. Fujiki K, Hotta Y, Murakami A, Yoshii M, Hayakawa M, Ichikawa T, Takeda M, Akeo K, Okisaka S, Kanai A. *Jpn. J. Hum. Genet* 1995;40:271–277. [PubMed: 8527802]
71. Sullivan LJ, Makris GS, Dickinson P, Mulhall LE, Forrest S, Cotton RG, Loughnan MS. *Arch. Ophthalmol* 1993;111:1512–1517. [PubMed: 8240107]
72. Yoshii M, Murakami A, Akeo K, Fujiki K, Saga M, Mizukawa A, Itoh J, Okisaka S, Yanashima K, Hotta Y, Kanai A, Oguchi Y. *Ophthalmic Res* 1998;30:1–10. [PubMed: 9483582]

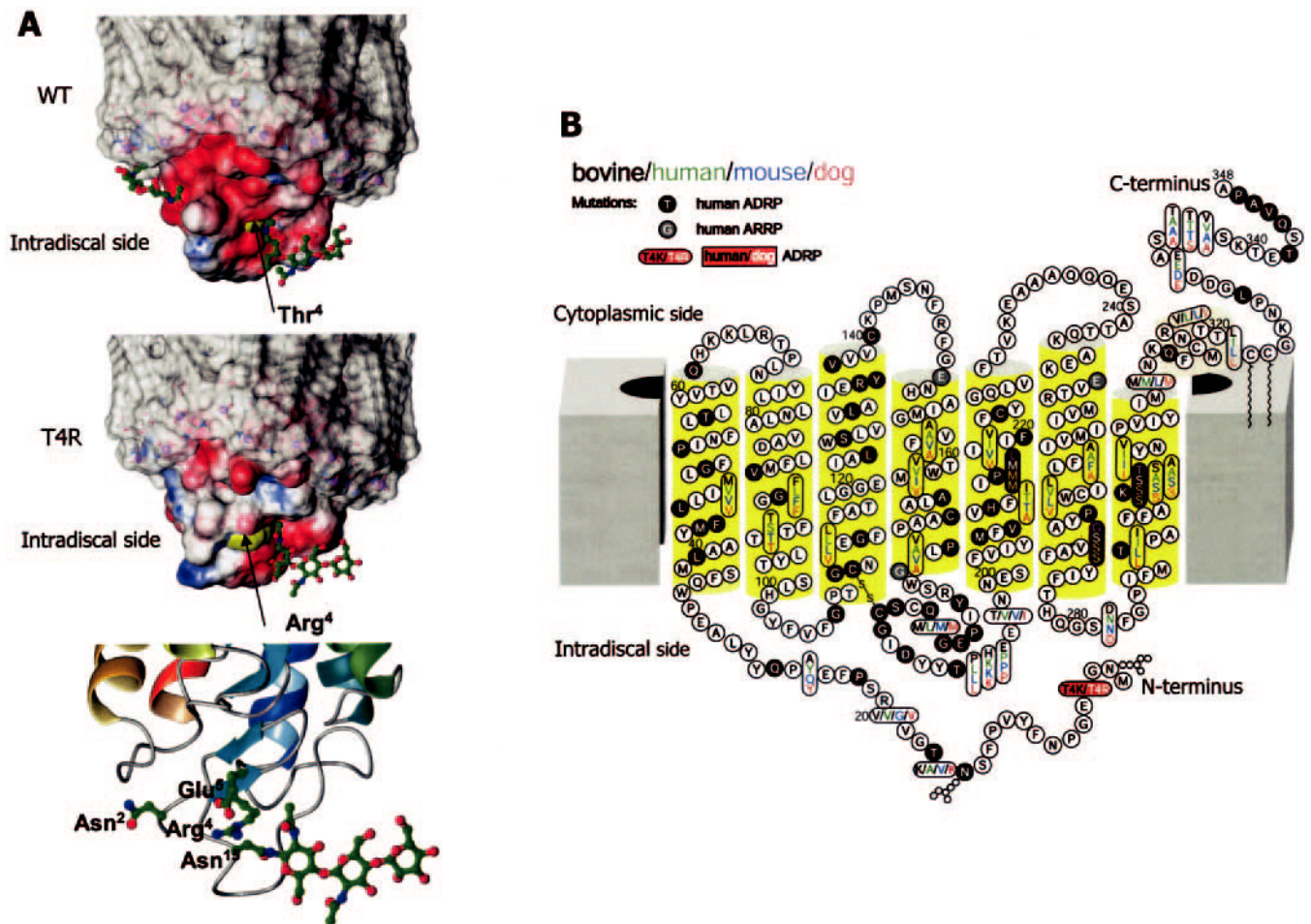


Fig. 1.
Models of WT and T4R Rho. *A*, three-dimensional models of WT (*upper panel*) and T4R mutant (*middle panel*) Rho embedded in phospholipid bilayers. The model of oligomeric WT Rho in the membranes was described previously (41), and it is based on the crystal structure of bovine Rho (8). Only the first shell of phospholipids is shown. The electrostatic potential is mapped onto the rhodopsin surface. *Red* denotes negatively charged areas, and *blue* denotes positively charged areas. The T4R mutation changes the charge distribution around Asn², making its surroundings positive and preventing glycosylation at this site. The electrostatic potential is nearly unaffected at the Asn¹⁵ site. *Lower panel*, detailed view of the intradiscal domain of T4R Rho. Arg⁴ likely forms an ion pair with Glu⁵. *B*, two-dimensional model of Rho for bovine (*black*), human (*green*), mouse (*blue*), and dog (*red*). Mutations associated with autosomal dominant RP (ADRP) are on a *black* background, whereas those associated with autosomal recessive RP (ARRP) are on a *gray* background. The T4R and T4K point mutations are shown on a *red* background. Note that T4R Rho found in dogs (22) resembles RP mutation T4K in man (16), possibly affecting glycosylation at position 2.

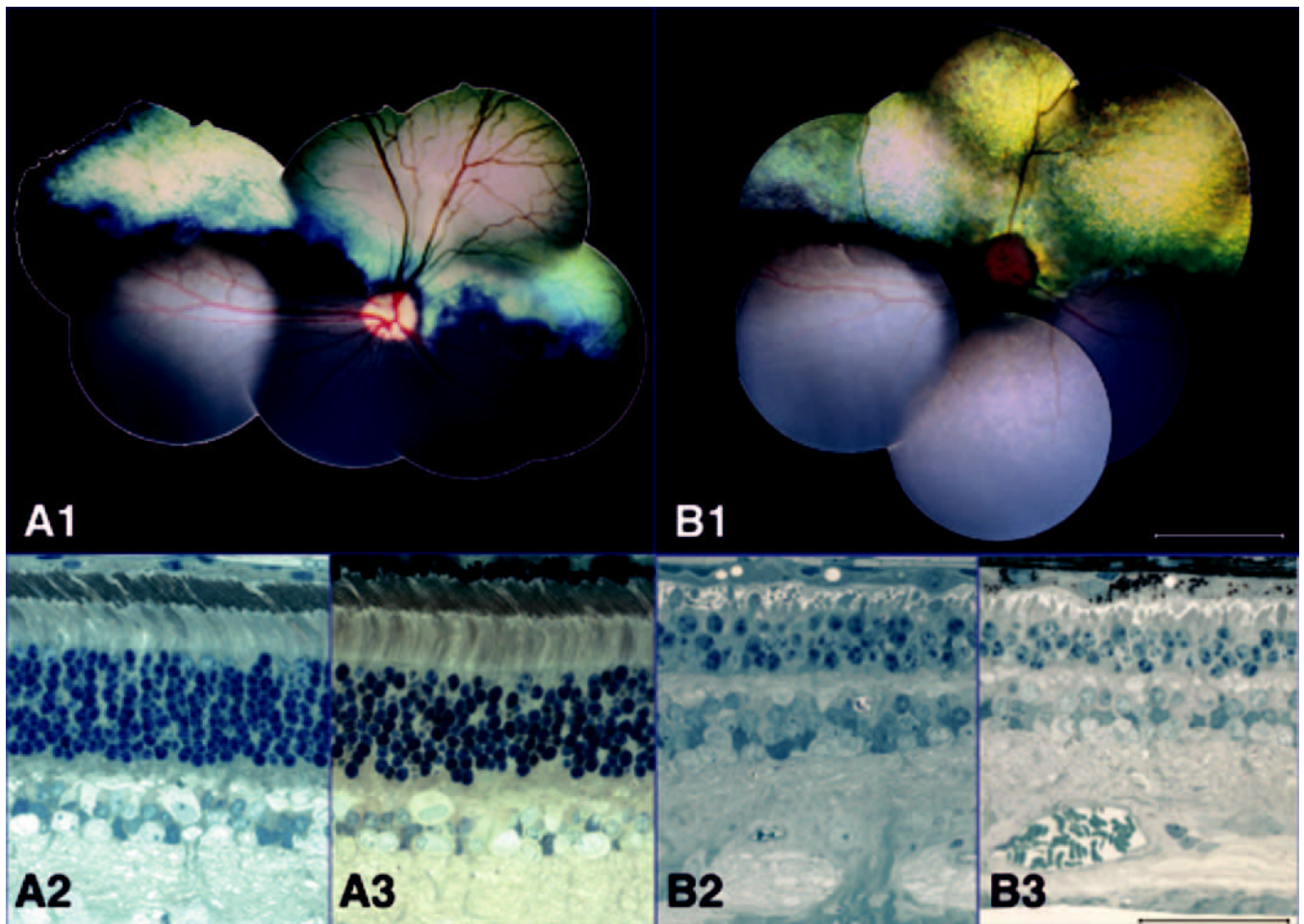


Fig. 2.
Fundus photography and retinal morphology of affected dogs. *A1*, photomontage of the interior posterior surface of the eyeball, including the retina, optic disc, macula, and posterior pole (fundus) of the left eye of an 8-month-old affected $RHO^{T4R/+}$ dog. The fundus is normal. *A2*, retinal morphology of the central superior (tapetal) region of the retina of the right eye of the same dog. *A3*, retinal morphology of the peripheral region of the same dog. The retina is uniformly normal morphologically. *B1*, fundus photomontage of the left eye of a 6.5-month-old $RHO^{T4R/+} RPE65^{-/-}$ double mutant dog. There is hyperreflectivity of the tapetal fundus (indicative of retinal thinning) and moderate vascular attenuation, changes typical of mid-stage progressive retinal atrophy. *B2* and *B3*, superior and inferior retinas, respectively, of a 6.5-month-old $RHO^{T4R/+} RPE65^{-/-}$ double mutant dog. Mid-stage outer retinal degeneration is present uniformly throughout the double mutant retina. *Scale bars* = 5.0 mm (*A1* and *B1*) and 50 μ m (*A2*, *A3*, *B2*, and *B3*).

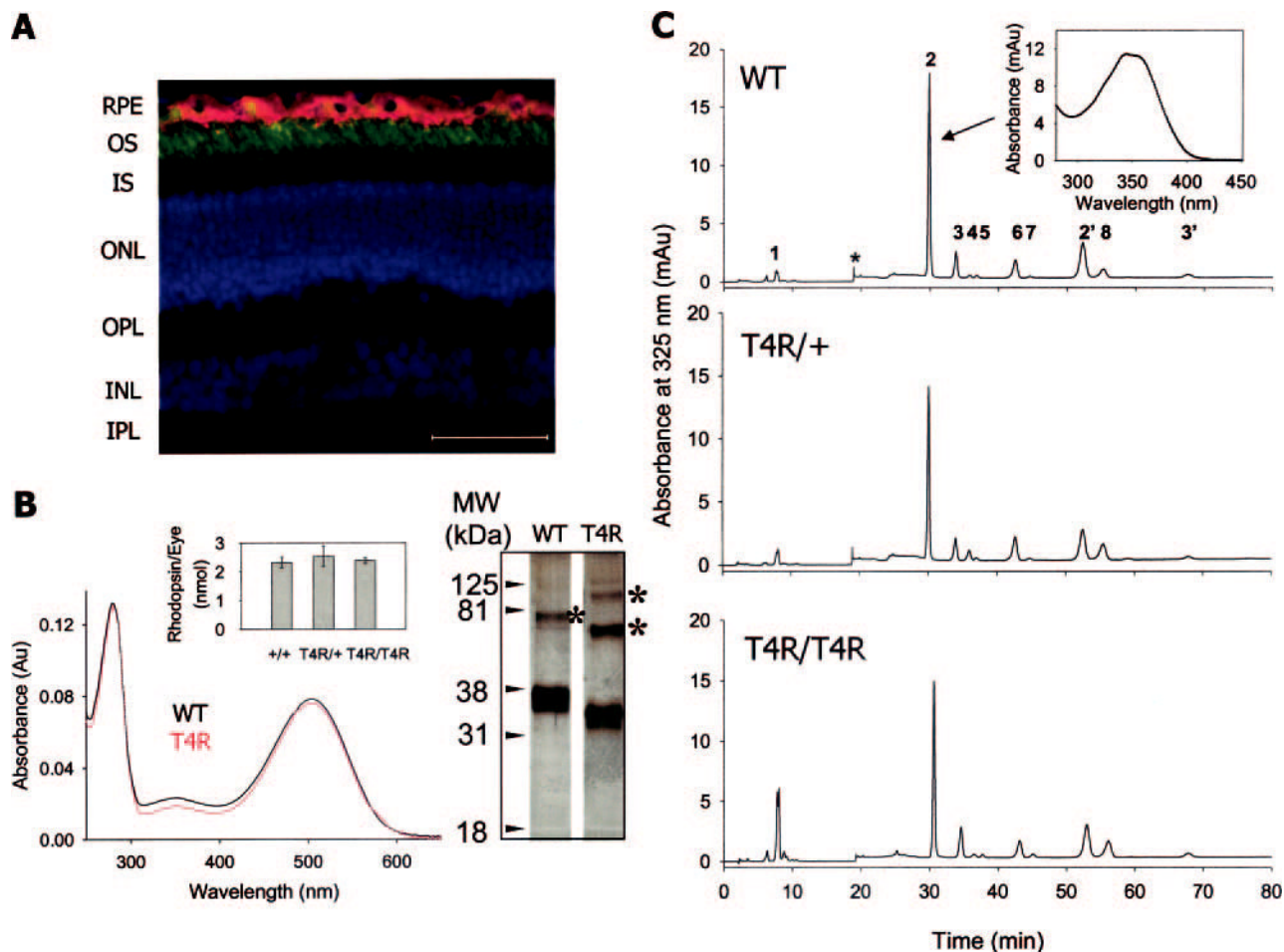


Fig. 3. Localization and quantification of Rho in the retina of a $RHO^{T4R/T4R}$ mutant dog and retinoid analysis. **A**, retinal immunocytochemistry of a frozen section from the right eye of a 3-month-old homozygous affected $RHO^{T4R/T4R}$ dog. Opsin is shown in *green*, and the retinal pigment epithelium protein RPE65 is in *red*. RPE, retinal pigment epithelium; OS, outer segment; IS, inner segment; ONL, outer nuclear layer; OPL, outer plexiform layer; INL, inner nuclear layer; IPL, inner plexiform layer. Nuclei were visualized by staining with Hoechst 33342 dye (*blue*). Scale bar = 50 μ m. **B**, UV-visible absorption spectra (*left panel*) and silver-stained SDS-polyacrylamide gel (*right panel*) of immunoaffinity-purified WT and T4R Rho. The *asterisks* indicate SDS-induced oligomers of Rho and the mutant. *Inset*, the amount of Rho solubilized in 1% DM, 150 mM NaCl, and 10 mM bis-tris propane (pH 7.5) from one retina of a WT, $RHO^{T4R/+}$, or $RHO^{T4R/T4R}$ dog. The amounts of Rho were measured in three independent experiments from which the standard deviations were calculated. The retinas were harvested from 3-month-old dogs for all three genetic backgrounds. *Au*, absorbance units. **C**, retinoid composition of WT, $RHO^{T4R/+}$, and $RHO^{T4R/T4R}$ dog retinas in the superior central region (one-sixth of the eye surface) analyzed by HPLC. *Peak 1*, all-*trans*-retinyl ester; *peak 2*, *syn*-11-*cis*-retinal oxime; *peak 3*, *syn*-all-*trans*-retinal oxime; *peak 4*, *syn*-9-*cis*-retinal oxime; *peak 5*, *syn*-13-*cis*-retinal oxime; *peak 6*, 11-*cis*-retinol; *peak 7*, all-*trans*-retinol; *peak 2'* and *3'*, *anti*-isomers of the corresponding compounds, respectively. The *asterisk* indicates influence from change of the solvent (for details, see "Experimental Procedures"). Proportional amounts of retinoid between genetic backgrounds were found in 3-mm retina punches or in extracts from whole eyes. *mAu*, milli-absorbance units.

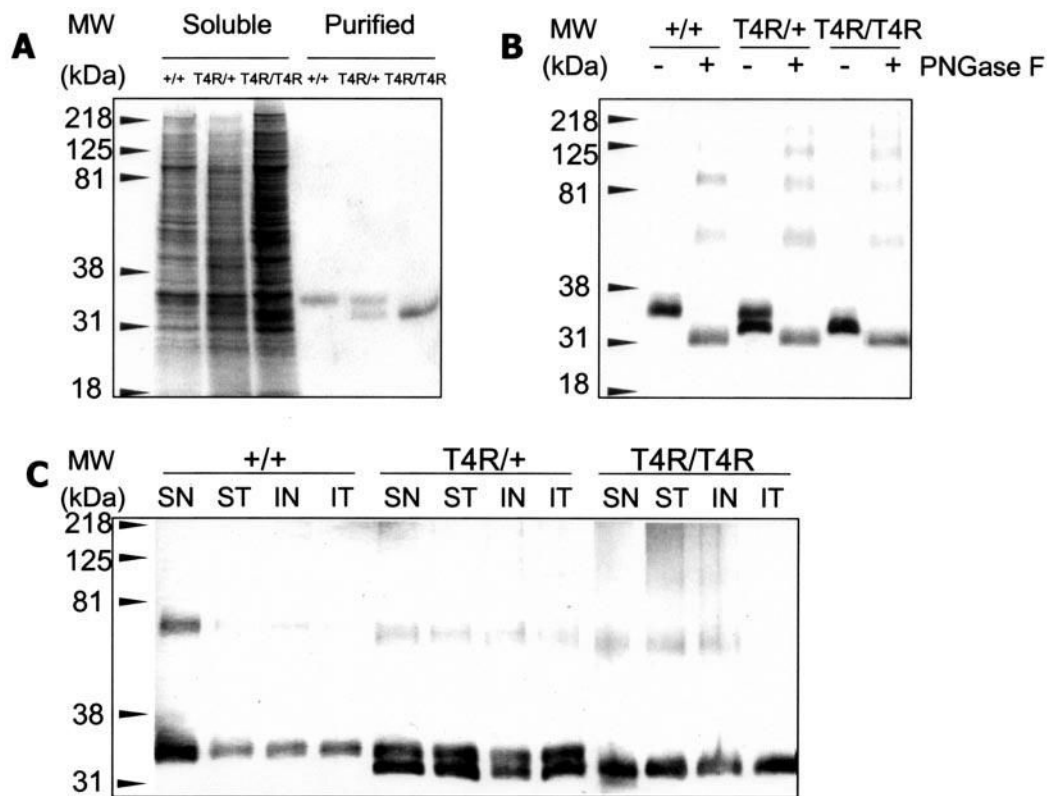


Fig. 4.

Glycosylation status of T4R Rho. *A*, glycosylation status of extracted and purified Rho from dogs of different genetic backgrounds with respect to Rho mutation. The Coomassie Blue-stained SDS-polyacrylamide gel shows supernatant solubilized in 1% DM (*left*) and immunoaffinity-purified Rho (*right*) from WT, $RHO^{T4R/+}$, and $RHO^{T4R/T4R}$ dog retinas. *B*, immunoblot of immunoaffinity-purified Rho. Rho from WT, $RHO^{T4R/+}$, and $RHO^{T4R/T4R}$ dog retinas before and after deglycosylation with peptide *N*-glycosidase F (*PNGase F*) was detected with anti-Rho C terminus antibody 1D4. *C*, immunoblot of Rho from different quadrants of WT, $RHO^{T4R/+}$, and $RHO^{T4R/T4R}$ dog retinas. Similar results were obtained in three to five independent experiments. *SN*, superior nasal; *ST*, superior temporal; *IN*, inferior nasal; *IT*, inferior temporal.

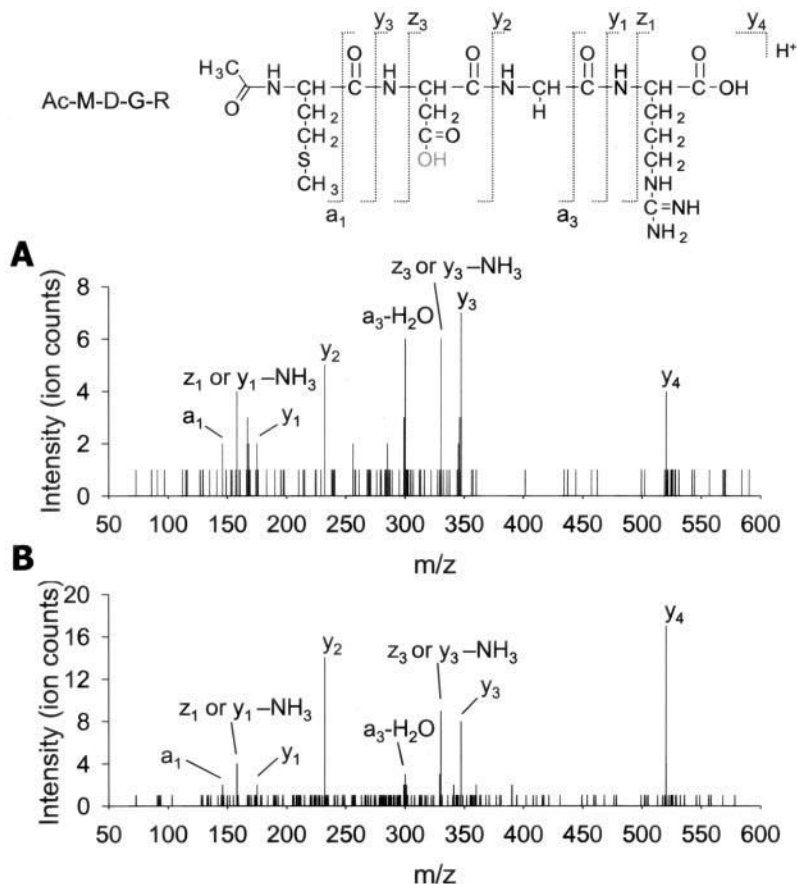


Fig. 5. **LC-MS/MS analysis of tryptic N-terminal peptides.** Shown are the results of analysis using the standard synthetic peptide Ac-MNGREGPNGYV (**A**) and immunoaffinity-purified T4R Rho (**B**). The expected product, Ac-MNGR, $[M + H]^+$ at m/z 519.2354, was not observed, but instead, its deaminated product, Ac-MDGR, $[M + H]^+$ at m/z 520.2184, was detected in both cases. Both MS/MS spectra of Ac-MDGR at m/z 520.2310 from the standard (**A**) and at m/z 520.1900 from T4R Rho (**B**) were nearly identical. The characteristic fragments for calculated m/z values are as follows: y_4 , 520.2184; y_3 , 347.1673; y_2 , 232.1404; y_1 , 175.1189; z_3 - or y_3 -NH₃, 330.1408; z_1 - or y_1 -NH₃, 158.0924; a_3 -H₂O, 300.0970; and a_1 , 146.0640. The structure at the top shows the fragmentation patterns of this tetrapeptide. The analysis was reproduced in two independent experiments. The deaminated residue is shown in gray.

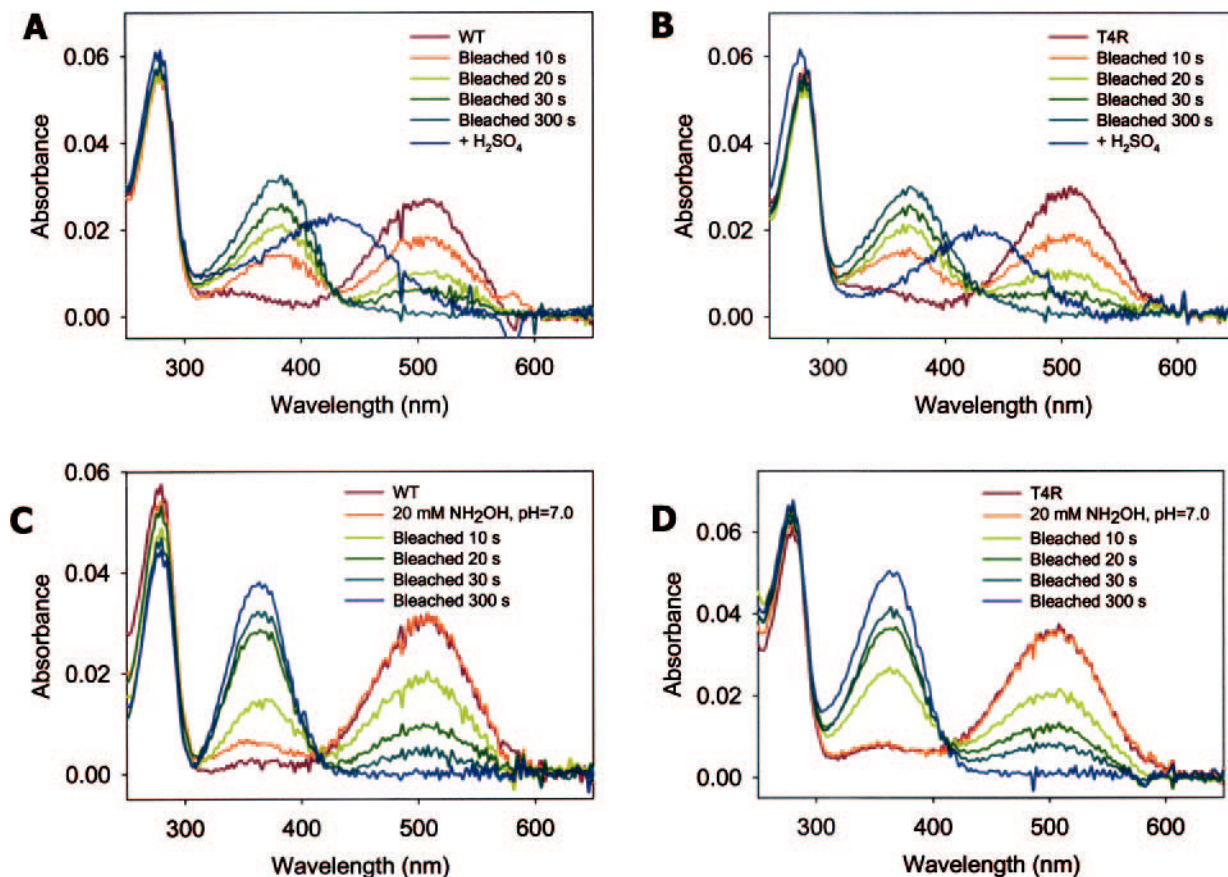


Fig. 6.

UV-visible spectra of WT and T4R Rho after bleaching. Immunoaffinity-purified WT Rho (A and C) and T4R Rho (B and D) were bleached for the indicated times without (A and B) or with (C and D) 20 mM neutral NH_2OH . In A and B, the pH of the samples was adjusted to 1.9 with H_2SO_4 to protonate the Schiff base. The bleaching of WT and T4R Rho was similar, whereas the amount of acid-trapped retinylidene-opsin was lower in the Rho mutant. Similar spectra were obtained in three independent experiments.

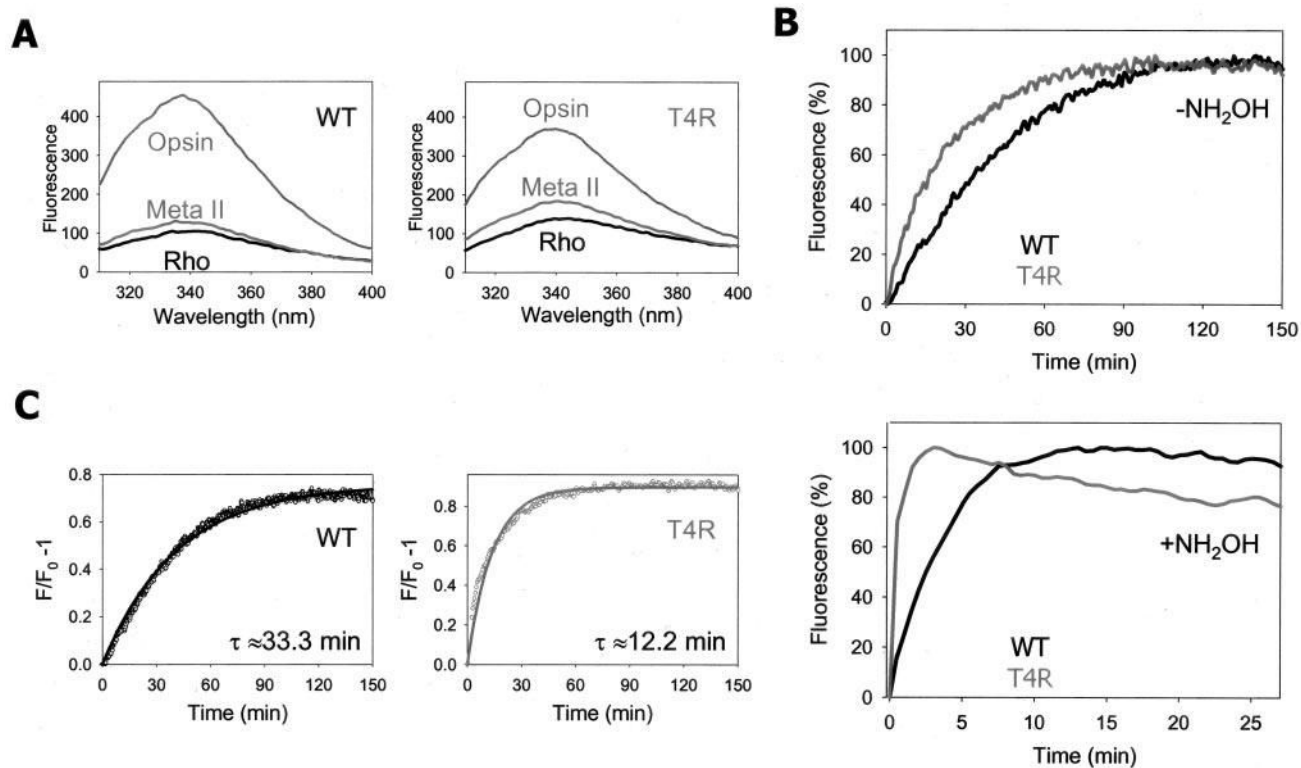


Fig. 7.
Meta II decay of WT and T4R Rho. *A*, shown are the fluorescence emission spectra of WT Rho (*left panel*) and T4R Rho (*right panel*) before (*black trace*), immediately after (*dark gray trace*), and after thorough (*light gray trace*) photobleaching. *B*, the decay of WT Rho (*black trace*) and T4R Rho (*red trace*) Meta II was recorded with (*lower panel*) or without (*upper panel*) 10mM NH₂OH at pH 6.0. Similar results were obtained in five independent experiments. *C*, the data from *B* without NH₂OH were fitted to a first-order reaction, which gives the relaxation times (τ) of WT Rho (*left panel*) and T4R Rho (*right panel*) Meta II as 33.3 and 12.2 min, respectively. Similar results were obtained in five independent experiments.



Fig. 8.
Stability of WT and T4R Rho. The stability of Rho was measured as a change in the UV-visible absorption spectra at its absorption maximum at 37 °C without (A) or with (B) 20 mM neutral NH₂OH. The results were plotted assuming 100% absorption at the initial point. Bovine Rho was used as a control for the NH₂OH sample. Similar results were obtained in three independent experiments.

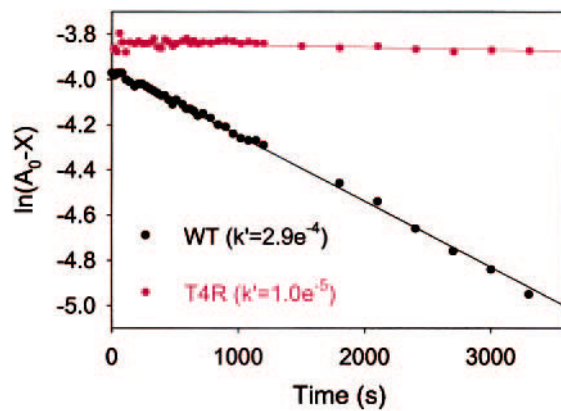


Fig. 9.

Regeneration of WT and T4R Rho in digitonin. 11-*cis*-Retinal was added in 50-fold excess to the purified opsins solubilized in 2% digitonin, 10 mM bis-tris propane, and 500 mM NaCl (pH 7.5). UV-visible spectra were recorded as a function of time, and the data were then fitted to a pseudo first-order reaction: $\ln(A_0 - X) = -k't + C$, where X is the absorbance at 500 nm at any given time and A_0 is the absorbance at 500 nm before Rho was bleached. WT opsin regenerated at a rate ~ 30 times faster than the T4R mutant. Regeneration reached the level of $\sim 70\%$ compared with the starting amount of Rho.

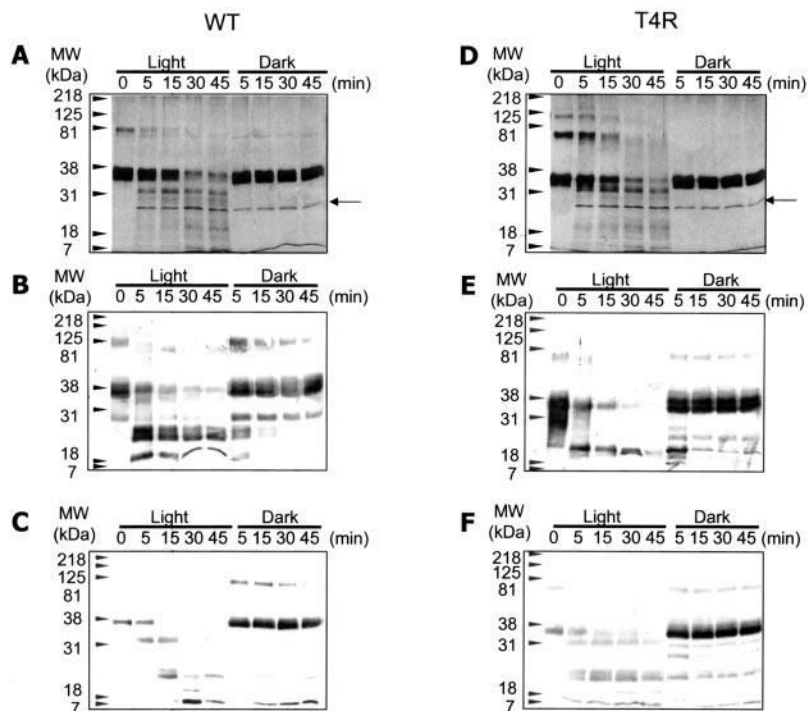


Fig. 10.
Limited proteolysis of WT and T4R Rho. At a 200:1 molar ratio of Rho to trypsin, immunoaffinity-purified WT (A–C) or T4R (D–F) opsin (*second through sixth lanes*) or Rho (*seventh through tenth lanes*) was trypsinized for the indicated times (0, 5, 15, 30, and 45 min) at room temperature. Opsin was generated from Rho by bleaching with a Fiber-Lite illuminator for 5 min at room temperature in the presence of 20 mM neutral NH_2OH . A and D, silver-stained SDS-polyacrylamide gels; B and E, anti-Rho N terminus antibody B6-30N immunoblots; C and F, anti-Rho C terminus antibody 1D4 immunoblots. The *arrows* indicates the trypsin band. Similar digestion patterns were obtained in three independent experiments.

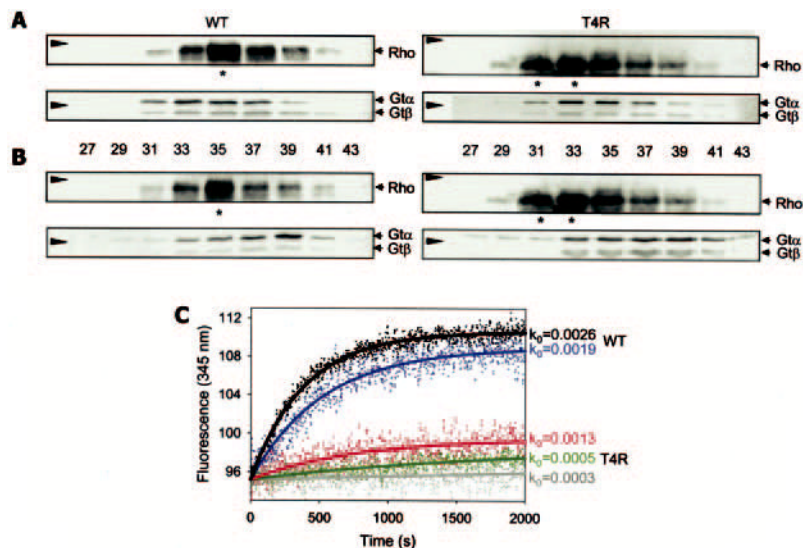


Fig. 11.

G_t activation assay with WT and T4R Rho*. *A* and *B*, G_t incubated with Rho* (see “Experimental Procedures”) was submitted to size exclusion chromatography, and the resulting fractions were examined by immunoblotting with anti-Rho C terminus antibody 1D4 (*upper panels*) or anti-Gα and anti-Gβ_t antibodies (*lower panels*). Fraction numbers are indicated. Similar results were obtained in three independent experiments. In *B*, GTPγS was present in the samples before loading onto the column. In *A* and *B*, the *arrows* inside the box represent a molecular mass marker of 38.5 kDa. The *asterisks* denote the fractions with the highest protein content. *C*, the intrinsic fluorescence G_t assay was performed with WT Rho at pH 6.0 (*black trace*) and pH 7.5 (*blue trace*) and with T4R Rho at pH 6.0 (*red trace*) and pH 7.5 (*green trace*) and upon incubation 800 s before addition of GTPγS at pH 7.5 (*gray trace*) at a 1:10 molar ratio of Rho to G_t. The apparent initial rates after curve fitting were calculated as follows: WT Rho at pH 7.5, $k_0 = 0.0026 \text{ s}^{-1}$; WT Rho at pH 6.0, $k_0 = 0.0019 \text{ s}^{-1}$; T4R Rho at pH 6.0, $k_0 = 0.0013 \text{ s}^{-1}$; T4R Rho at pH 7.5, $k_0 = 0.0005 \text{ s}^{-1}$; and T4R Rho at 800 s > $\tau_{\text{Meta II}}$ at pH 7.5, $k_0 = 0.0003 \text{ s}^{-1}$. The initial G_t activation rates were calculated from three independent experiments under each condition.